In Vivo Brillouin Analysis of the Aging Crystalline Lens

Sebastien Besner,[1,2] Giuliano Scarcelli,[1–3] Roberto Pineda,[4] and Seok-Hyun Yun[1,2,5]

[1]Wellman Center for Photomedicine, Massachusetts General Hospital, Cambridge, Massachusetts, United States
[2]Department of Dermatology, Harvard Medical School, Boston, Massachusetts, United States
[3]Fischell Department of Bioengineering, University of Maryland, College Park, Maryland, United States
[4]Department of Ophthalmology, Massachusetts Eye and Ear Infirmary, Boston, Massachusetts, United States
[5]Harvard-MIT Health Sciences and Technology, Cambridge, Massachusetts, United States

Correspondence: Giuliano Scarcelli, 65 Landsdowne Street, Cambridge, MA 02139, USA; scarc@umd.edu.
Seok-Hyun Yun, 65 Landsdowne Street, Cambridge, MA 02139, USA; syun@hms.harvard.edu.

Submitted: June 17, 2016
Accepted: August 3, 2016

Citation: Besner S, Scarcelli G, Pineda R, Yun SH. In vivo Brillouin analysis of the aging crystalline lens. *Invest Ophthalmol Vis Sci*. 2016;57:5093–5100. DOI:10.1167/iovs.16-20143

Purpose. To analyze the age dependence of the longitudinal modulus of the crystalline lens in vivo using Brillouin scattering data in healthy subjects.

Methods. Brillouin scans were performed along the crystalline lens in 56 eyes from 30 healthy subjects aged from 19 to 63 years. Longitudinal elastic modulus was acquired along the sagittal axis of the lens with a transverse and axial resolution of 4 and 60 μm, respectively. The relative lens stiffness was computed, and correlations with age were analyzed.

Results. Brillouin axial profiles revealed nonuniform longitudinal modulus within the lens, increasing from a softer periphery toward a stiffer central plateau at all ages. The longitudinal modulus at the central plateau showed no age dependence in a range of 19 to 45 years and a slight decrease with age from 45 to 63 years. A significant intersubject variability was observed in an age-matched analysis. Importantly, the extent of the central stiff plateau region increased steadily over age from 19 to 63 years. The slope of change in Brillouin modulus in the peripheral regions were nearly age-invariant.

Conclusions. The adult human lens showed no measurable age-related increase in the peak longitudinal modulus. The expansion of the stiff central region of the lens is likely to be the major contributing factor to age-related lens stiffening. Brillouin microscopy may be useful in characterizing the crystalline lens for the optimization of surgical or pharmacological treatments aimed at restoring accommodative power.

Keywords: lens, biomechanics, Brillouin microscopy

Although individuals usually recognize presbyopia symptoms only after the age of 40 years, the change in the accommodative amplitude is a lifelong process decreasing almost linearly from the age of 10 to 60 years.[1] The etiology of presbyopia is not completely understood, but two age-related biomechanical changes have been hypothesized as a root cause of this problem. One is the aging of the ciliary muscle that exerts the force required to vary the shape of the crystalline lens[2,3]; the other is the stiffening of the lens itself with increasing age.[4] Recent evidence from primates and human studies indicates that muscle function is normal beyond the onset of presbyopia.[5] Therefore, it is believed that the age-related stiffening of the crystalline lens and its resulting increased resistance to deformation are the dominant processes causing the loss of accommodation.[6–9]

The deformability of the lens is typically quantified by the elastic moduli such as Young's or shear modulus. However, these parameters are difficult to measure for the crystalline lens because of its small size and spatially varying modulus values. The published data on the mechanical properties of the human lens have large variability. The Young's moduli of human cadaver lenses, measured by conventional mechanical tests, vary over a wide range from 20 Pa to 2 MPa.[10] A broad range of values is also found in the age-related lens stiffening in which a variety of values from negligible increases up to a factor of 10,000 were reported.[8,9,11–17] Data on the regional distribution of elastic modulus within the lens have also been inconsistent. Some studies have indicated that the nucleus should be softer than the cortex up to an age of 30 to 50 years,[11,15–17] but others measured comparable elasticity[12] or stiffer nucleus.[18,19] Ex vivo rheological assessment is also compounded by postmortem changes of the structural and mechanical properties of the lens tissue.[20,21]

Brillouin microscopy is a new imaging modality based on spontaneous Brillouin light scattering in samples. Brillouin scattering arises from acoustic phonons. Acoustic phonons are equivalent to the wave propagation of thermodynamic fluctuations of the medium, which produces a periodic modulation of refractive index to cause light scattering. The light scattered from the traveling index modulation experiences a Doppler frequency shift equal to the frequency of the phase-matching acoustic phonon. From the Brillouin frequency shift, one can measure longitudinal modulus, a type of elastic modulus different from but related to Young's and shear moduli. Brillouin microscopy is similar to acoustic microscopy or ultrasounds[22,23] in a sense that their principle involves the measurement of acoustic propagation speeds or longitudinal modulus, but they differ in that Brillouin microscopy does not require ultrasound transducers and offers much higher optical resolution.[24–27] Optical coherence elastography has been used to measure the overall stiffness of crystalline lenses,[28] but to date high-resolution analysis of the spatial distribution of elastic modulus has not been demonstrated.

Investigative Ophthalmology & Visual Science

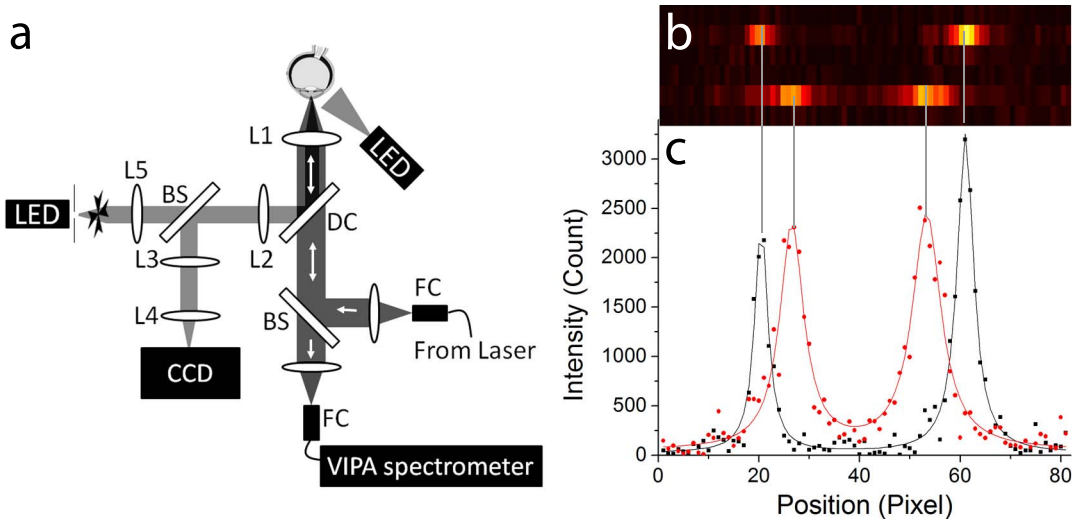

Figure 1. (**a**) Schematic representation of the Brillouin confocal in vivo microscope. (**b**) Raw EMCCD output of the VIPA spectrometer showing the vitreous humor (*top*) and lens nucleus (*bottom*) at an integration time of 0.2 seconds and a laser power of 2 mW. The two peaks represent the stoke shift and the antistoke shift of the following laser order. (**c**) 2-Lorentzian peak fit (*solid line*) of the raw imaging data (*points*) along the Brillouin spectral line for vitreous humor (*black*) and lens nucleus (*red*).

Brillouin microscopy revealed a marked age-related stiffening of the lens nucleus between young and old mice in vivo.[24] A previous study on human cadaver lenses showed no statistically significant change in the longitudinal modulus of the lens nucleus and cortex.[29] We have developed a clinically viable, safe Brillouin imaging system using low-power near-infrared (NIR) light (Besner S, et al. *IOVS* 2013;54:ARVO E-Abstract 4270). Here, we describe the results of our first human study to measure the Brillouin longitudinal modulus of the crystalline lens in healthy humans across an age range from 19 to 63 years.

Materials and Methods

Research Subjects

All participants received a detailed explanation of the study and signed an informed consent form approved by the Partners Human Research Committees (institutional review board), in accordance with the principles embodied in the Declaration of Helsinki. Brillouin sagittal profiles were acquired in 56 eyes of 30 healthy subjects, age 19 to 63 years old (mean age: 36 ± 13 years). Exclusion criteria included cataracts, allergy to ophthalmic medications, severe refractive abnormalities, occludable narrow angles or other pathologies that preclude safe dilation, systemic disease, and previous refractive surgery.

In Vivo Brillouin Confocal Microscope

Figure 1 schematically represents the confocal Brillouin microscope used in this study. The system employed a 780-nm tunable laser diode (DL-Pro; Toptica Photonics, Munich, Germany) with an optical power of 2 mW on the cornea surface. The laser light was focused by a ×5 infinity-corrected objective lens (NA = 0.1; Mitutoyo America, Aurora, IL, USA) with a long working distance of 34 mm. The beam size at the focus was approximately 4 μm laterally (*x-y*) and 60 μm (*z*) axially. The focus was scanned along axial lines by translating the objective with a motorized stage (T-LSM25; Zaber Technologies, Vancouver, BC, Canada). A wide-field video camera was used to track the pupil and to control the *x-y* position of the scan axis. A Maltese cross fixation target was used on a modified Badal optometer to fix the vergence of the eye during axial scans.

The collected Brillouin backscattered light was spectrally dispersed by a spectrometer consisting of a two-stage virtually imaged parallel array (VIPA) device and imaged onto an electron-magnification charged coupled device (IXon Du-897; Andor Technologies, Belfast, Northern Ireland). The details of the spectrophotometer design can be found elsewhere.[30–32] Figures 1b and 1c report typical raw Brillouin spectra for the human vitreous humor and the lens nucleus, and the 2-Lorentzian peak fit used to determine Brillouin frequency shifts. The setup used LabVIEW (National Instruments, Austin, TX, USA) for real-time operations, including hardware control, laser-to-eye position registration, image processing, and display of raw spectrometer output and Brillouin line-scan profiles.

Brillouin Imaging Protocol

During Brillouin scans, the subject was asked to stare at the fixation target through the objective lens. The visual stimulus was set at a far point (infinity) with correction of the vergence to compensate the refractive error of the eye. A chin and front rest were used to reduce subject's motions. The axial scanning speed was adjusted between 150 and 850 μm/s for an EMCCD integration time of 0.1 to 0.4 second, taking into account the individual subject's ability to fixate and stay still. Typical axial scan durations ranged between 10 and 20 seconds at a laser power of 2 mW. In initial scans, low-resolution Brillouin axial profiles of the whole anterior segment were taken to locate the interface of the posterior cornea, anterior and posterior lens capsule, and anterior and posterior lens nucleus with an accuracy of approximately 120 μm. The measured distances were then included in an iterative eye propagation model based on a full Gullstrand eye model[33] to determine the actual focal depth within the eye. Following this initial procedure, high-resolution scans along the sagittal axis of the lens were performed with a step size of 60 μm, the same as the axial resolution of our system. A minimum of 10 scans were performed on each eye to confirm reproducibility of the scan data. Scans with significant motion artifact, as determined by

the eye registration system, were removed from the analysis. The valid scan profiles were overlaid and averaged.

Laser Safety

The laser power of 2 mW is 63 times lower than the maximum permissive exposure defined by the American National Standards Institute for retinal hazard[34] and 16 times lower than the guideline of the International Committee on Non-Ionizing Radiation Protection standards for the lens and cornea thermal hazards.[35,36] None of the subjects expressed any discomfort, pain, or vision problems during or after the imaging session. The laser light was seen as a diffuse faint-red color, barely visible on top of the fixation target projection. For the first 10 subjects, comprehensive eye examinations were performed at Massachusetts Eye and Ear Infirmary before and 6 months after scan sessions. No adverse effects to the subjects' eyes were identified.

Brillouin Longitudinal Modulus

The Brillouin shift was obtained from the spacing between the Stokes (left peak) and anti-Stokes shift (right peak). For accurate calibration, the free spectral range and spectral dispersion of the spectrometer were determined from the measured Brillouin spectra of two known materials, water and poly(methyl methacrylate) plastic, immediately before or after each human imaging session.[37,38] This calibration step allowed subpixel localization of the peak central position even in the presence of the typical drifts in the laser frequency and spectrometer alignment. The measurement error in Brillouin shifts was approximately 16 MHz at a laser power of 2 mW and an integration time of 0.2 second. The long-term frequency stability of the measurement was better than 16 MHz, as estimated from the standard deviation (SD) in repetitive measurements of test materials over 30 days.

The Brillouin longitudinal modulus (M') was calculated from the Brillouin shift (Ω) according to the following relation:

$$M' = \frac{\rho \Omega^2 \lambda^2}{4n^2 \sin^2(\theta/2)},$$

where ρ is the mass density, λ (780 nm) is the optical wavelength in air, n is the refractive index, and θ (180 degrees in our experimental condition) is the angle between the incident and scattered light. The refractive index and density of the tissue are spatially nonuniform within the lens; however, the ratio of ρ/n^2 is approximately constant at 0.5636 g/cm^3 with a variation of less than 1% throughout the lens.[24]

Regional Dependence of the Brillouin Longitudinal Modulus

To quantify the regional variation of lens elasticity, the obtained sagittal profiles were fitted using a general power law model[39,40]:

$$M = M_{\max} - \Delta M \left(\frac{|x - x_c|}{L} \right)^{\gamma}.$$

The central position x_c and thickness L were obtained from the Brillouin axial profiles, and the peak modulus $M_{\max}$, the amplitude of variation ΔM, and the exponents γ were used as fitting parameters. Separate fits were performed for the anterior cortex, anterior nucleus, posterior nucleus, and posterior cortex. For the plateau region fit, the inner region of the lens with the top 50% value of M was used to accurately reproduce the flat central region and the transitional region between the nucleus and the cortex (see Fig. 2). In this central region, x_c is the lens center, and L is the half lens width of this top 50% region. For the peripheral regions, all points lower than 98% of the peak longitudinal modulus were used in the fit. In these regions, x_c was the axial position at the 98% value, and L was the thickness of the anterior or posterior cortical region. The exponent γ is a geometric factor describing the shape of the lens's modulus profile (e.g., a parabolic profile for $\gamma = 2$, and bell-shaped profiles at higher γ values).

Donor Tissue and Dissection Protocol

Ex vivo measurements were conducted on 14 human eyes obtained from two young donors (mean age: 24 ± 2 years), and five old donors (mean age: 59 ± 6 years). The human donor eyes were obtained from the National Disease Research Interchange (Philadelphia, PA, USA), and used in compliance with the guidelines of the Declaration of Helsinki for research involving the use of human tissue. To limit postmortem swelling, the lens was surgically extracted from the eye at the donor agency and immediately stored in mineral oil at 4°C before shipment. The mean postmortem preservation time was 7.8 ± 1.8 hours. On arrival, the ciliary body and lens capsule were carefully removed by making a small incision at the edge of the equatorial plane and by peeling out the capsule with surgical tweezers. Eight lenses were dissected into thin disks, and Brillouin microscopy and shear rheometry were performed on each disk. For dissection, the lens was cut with a scalpel in 1.5-mm-thick layers with cutting plane perpendicular to the equatorial plane. Then, from each layer, 4-mm disks were extracted by using a biopsy punch and then immediately stored in a small Petri dish filled with mineral oil. Ten or more disks were retrieved from each lens. The duration of the whole dissection procedure generally took approximately 20 minutes. For the other six lenses, the whole lenses were characterized with three-dimensional-scan Brillouin imaging and shear rheometer without dissection; the results of this analysis were consistent with the findings obtained with the dissection approach, but the details will be reported elsewhere.

Ex Vivo Comparison Between Brillouin and Shear Rheometry

Brillouin measurements were performed right after dissection. For each lens piece, a two-dimensional map (typically 40 × 40 points) in the central equatorial/sagittal plane was obtained by moving the sample with a three-axis translation stage (H117; Prior Scientific, Fulbourn, Cambridge, UK). From the map, the average value of the measured data was calculated, which represents the Brillouin longitudinal modulus of the sample. After Brillouin measurements, all lens samples were stored at 4°C, and allowed to thermalize at room temperature 20 minutes before rheometry measurements. For shear rheometry, a standard stress-controlled rheometer was used (AR-G2; TA Instruments, New Castle, DE, USA) with 8-mm diameter parallel plates, with a precompression of approximately 100 μm, frequency sweeps from 0.1 to 10 Hz with 0.1% strain amplitude. The data reported here refer to the shear modulus measured at approximately 0.2 Hz. All measurements were completed within 36 hours postmortem.

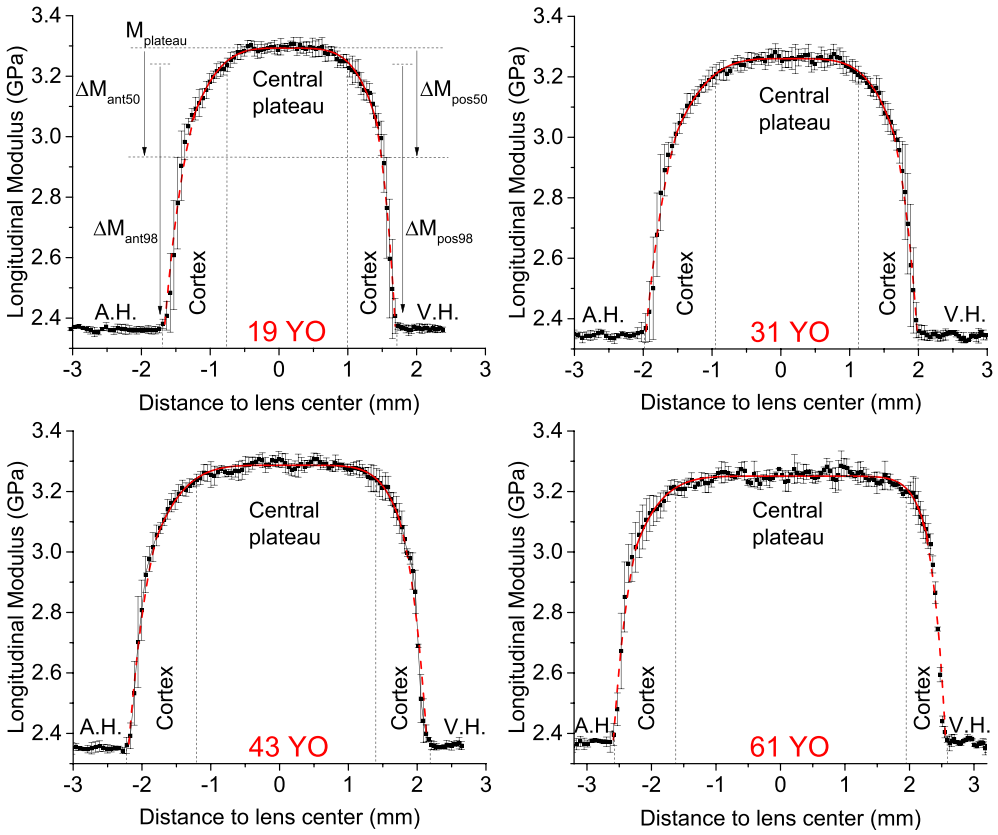

Figure 2. Representative Brillouin sagittal profiles in 19-, 31-, 43-, and 60-year-old human lenses showing the aqueous humor (A.H.), the vitreous humor (V.H.), the lens cortex, and central plateau. The central plateau is defined as the top 98% value in longitudinal modulus. The *points* and *error bars* represent the mean and SD of successive scans taken along the sagittal axis. Also shown is the definition of the different parameters of the power fit function.

Results

Regional Dependence of Lens Longitudinal Modulus

Figure 2 shows four representative axial profiles of Brillouin modulus obtained from 19-, 31-, 43-, and 61-year-old subjects. All measured profiles and fitting results are presented in Supplementary Fig. S1. In all subjects, the Brillouin frequency shifts of the aqueous and vitreous humors were equal within the instrument accuracy. Brillouin longitudinal modulus increased steeply in the lens periphery but moderately in the lens center. Based on the fitted profiles, we defined a central plateau region as the inner portion of the lens with the top 98% value in longitudinal modulus, and a peripheral region as the remaining outside of the central plateau region. The central plateau region corresponds, approximately, to the anatomical lens nucleus; the peripheral region includes the anterior and posterior lens cortices.

Intrasubject and Intersubject Variability

Figures 3a and 3b show several examples of sagittal Brillouin profiles taken from right (dashed line) and left (solid line) eyes of the same subject in young (Fig. 3a) and old (Fig. 3b) volunteers. The difference in the mean longitudinal elastic modulus of the central plateau region between the left and right eyes showed no statistically significant difference or the difference was smaller than the instrument accuracy. On the other hand, grouping individuals in age-matched subjects (±1.5 years), we found an intersubject variability of 57 ± 46 MHz, which is approximately three times larger than the system spectral resolution.

Age-Related Variations of Longitudinal Modulus

Figure 4 shows the age-related variations in thickness for the whole lens and for the different regions of the lens as previously identified on the base of their longitudinal modulus. A linear increase of the whole lens thickness at a slope of 32 ± 3 μm per year was found, and is consistent with previous measurements by Scheimpflug imaging, MRI, ultrasonography, and optical coherence tomography (Birkenfeld J, et al. *IOVS* 2015;56:ARVO E-Abstract 3566).[41,42] Importantly, the increase in the lens size was entirely due to a growth of the stiff central region (slope of 31 ± 3 μm/y); the thickness of the peripheral softer regions being constant with age. The mean thickness of the anterior peripheral region was 1.0 ± 0.2 mm, slightly greater than the mean thickness of the posterior peripheral region of 0.71 ± 0.13 mm.

Figure 5 shows the magnitudes of maximal Brillouin longitudinal modulus at the center of the lens and the minimal longitudinal modulus at the interfaces with the aqueous humor and vitreous. The minimal longitudinal modulus showed no statistically significant age dependence and had an identical average value of 2.36 ± 0.02 GPa in both the anterior and posterior sides. Also, the longitudinal modulus of the central plateau did not show statistically significant age dependence in the age range of 19 to 45 years. Beyond age 45, however, a small decrease in the longitudinal modulus of the central plateau was observed at a rate of –4.5 ± 1.4 MPa per year.

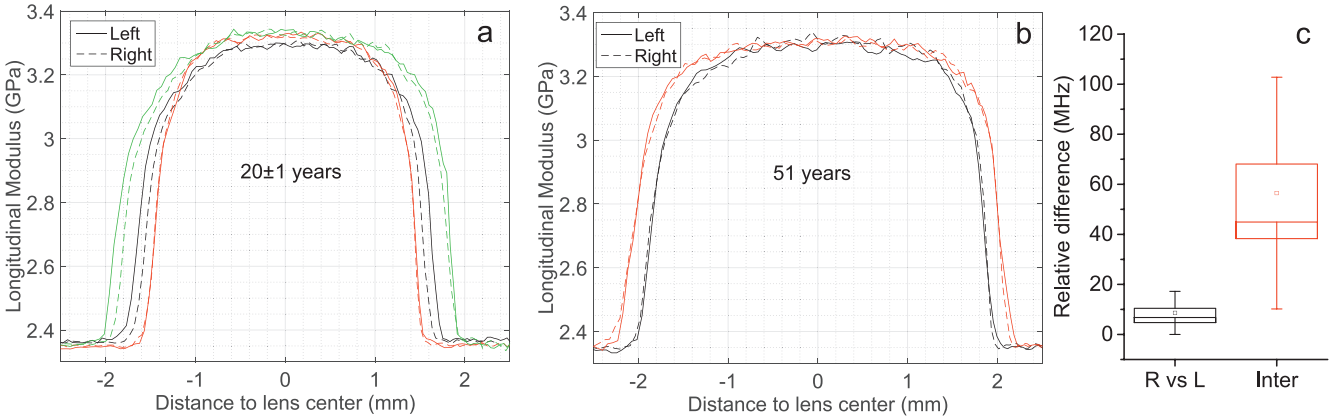

Figure 3. Intra- and intersubject variability. (**a**) Brillouin sagittal profiles of the left and right eyes of three individuals in an age range of 21 ± 1. (**b**) Comparison of the left and right eyes in two 51-year-old subjects. (**c**) The relative difference in the mean longitudinal modulus observed in the central plateau between the left and right eyes in the same subject and between subjects within an age-window of 3 years (*Inter*). The *box and whisker* represent the SE and the SD observed in all subjects.

Figure 6 shows the exponent γ obtained from the fitting of the anterior and posterior plateau regions. The γ parameter increased with the subject age significantly ($P < 0.001$) in a linear regression analysis, which is consistent with the observed flattening of the central region and an increase of the gradient at the transition between the central and peripheral regions. Figure 7 shows the Brillouin profiles in the peripheral regions. The γ parameters of the posterior and anterior regions were age-independent. The posterior region showed slightly greater γ than the anterior region.

Ex Vivo Comparison to Shear Rheometry

To compare the Brillouin longitudinal moduli with traditional shear moduli, we used ex vivo lens tissues cut into small pieces. Figure 8 shows the quasistatic shear modulus and the Brillouin longitudinal modulus along the equatorial direction. In both young and old lenses, we found an increase of the elastic modulus from the lens periphery toward the lens center. The variability within the same layer represents the intrinsic variations of shear and longitudinal moduli of lens tissues in the equatorial and sagittal axes. In young lenses, the measured quasistatic shear modulus ranged from 0.20 to 10.3 kPa, whereas the Brillouin modulus varied from 2.81 to 3.11 GPa. In old lenses, shear moduli ranged from 0.36 to 19.2 kPa, whereas Brillouin moduli ranged from 2.91 to 3.27 GPa, respectively. The six to seven orders of magnitude difference between shear and longitudinal moduli is well expected from the incompressibility of water and consistent with previous results.[44] Nevertheless, the correlation between Brillouin moduli and shear moduli is strong ($P < 0.05$ in linear regression analysis for all lenses analyzed).

Discussion

In this article, we have reported measurements of the mechanical properties of the aging human crystalline lens in vivo, for the first time to our knowledge. In particular, the high spatial resolution of Brillouin microscopy enabled us to characterize the spatial distribution of the longitudinal modulus within the crystalline lens. We found that, throughout all ages, the central portion of the lens is stiffer than the periphery. This result was confirmed by the ex vivo experiments, where we compared Brillouin moduli to shear moduli measured by traditional gold-standard shear rheometry. Our result is consistent with findings based on previous

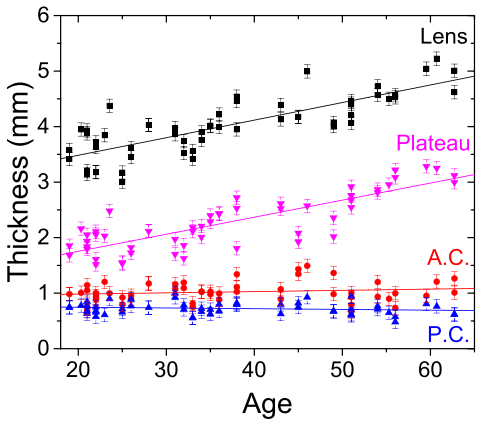

Figure 4. Variation of the human lens anterior cortex (A.C.), posterior cortex (P.C.), central plateau, and overall lens thickness with age. The *error bars* represent the instrument's thickness accuracy of 120 μm, which is a conservative assumption equal to twice the optical resolution of the Brillouin microscope and accounting for the accuracy in the two interfaces localization.

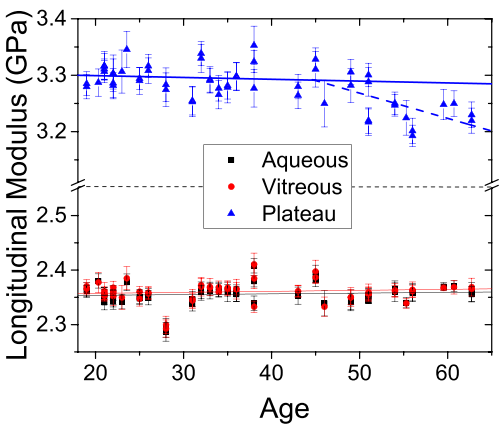

Figure 5. Variation of the Brillouin longitudinal modulus with age in aqueous humor, vitreous humor, and lens plateau. The *error bars* represent the SD within each eye subregion. For the plateau region, linear regressions for age younger than 45 years (*solid line*) and older than 45 years (*dashed line*) are shown.

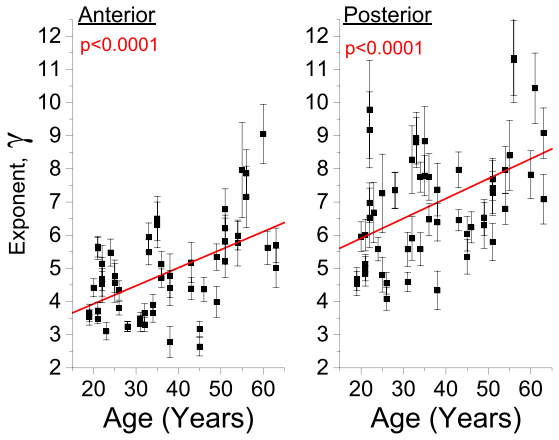

FIGURE 6. Variation of the power law exponent for the anterior and posterior region within the slowly varying central region of the lens. The *error bars* represent the 95% confidence bound of the fit coefficients.

Brillouin scattering experiments,[21,24,29,44,45] bubble-based acoustic radiation force,[19,46] and conical probe indentation,[18] in which the elastic modulus in the nucleus was always larger than in the cortex in both animals and human samples. However, these results do not agree with other experiments using spinning platforms and localized small probes in which the nucleus was found to be softer than the cortex in human lenses at ages up to 30 to 50 years old.[11,15–17] A softer nucleus at such age is difficult to explain, considering that elastic modulus typically increases with protein concentration. In preteenage lenses, the protein content within the nucleus is already much higher than the cortex.[47] Furthermore, the maximal compaction, leading to a constant protein concentration with age, is already completed in the center of the lens somewhere in the 20s.[43]

In terms of age-related trends, we did not find a statistically significant change of the peak longitudinal modulus with age in the range of 19 to 45 years, a period over which the accommodation power gradually decreases. Instead, the most prominent age-related change was the expansion and flattening of the central stiff plateau. By the age of 60 years, the sagittal thickness of the central plateau reached 3.2 ± 0.12 mm, a size in agreement with the four nuclear zones consisting of the embryonic, fetal, juvenile, and adult nuclei isolated by lyophilisation or hydrodissection.[48] Interestingly, no statistically significant age-related differences were found in the axial gradient of modulus in the peripheral regions. This may provide insights into the production of new lens fibers and their distribution and compaction.[49] Our data do not appear to support a notion that a "massive" increase of lens modulus is the main contributor to the age-related loss of accommodation.[11,15–17] Rather, the data point to the existence of other factors, such as the changes in lens shape.[42,47,50–55]

To estimate the actual elastic properties of the lens, it is necessary to convert the measured longitudinal modulus values to shear modulus. Although we have observed strong correlations (Fig. 8), a more detailed quantitative analysis is required. A more in-depth mechanical analysis of the lens will benefit from a volumetric Brillouin image, beyond an axial profile, of the lens. With the given experimental data, we estimate an approximately 2-fold increase in the overall stiffness of the lens from 19 to 45 years, which is consistent with previous ex vivo data.[8,56]

It is also worthwhile to note the apparent similarity between the profiles of longitudinal modulus and typical protein distributions that were previously obtained by optical techniques, and ultrasound.[39,43,47,57] This similarity provides insights into the relationship between the ultrastructure and the mechanical modulus of the lens tissues. In particular, the γ-crystallins are thought to enhance water expulsion by creating an extended network of alternately charged groups at their surface and creating a large number of molecular electrostatic dipole moments.[58] In humans, the relative protein proportion of the α-, β-, and γ-crystallins stays constant with age within the nucleus.[20] In contrast, in rodents, the γ-crystallins continue to be synthesized throughout life and thus may lead to a more extensive water loss with age.[59] Hence, one would expect the maximal compaction to saturate in humans in the nuclear region, whereas it should increase for rodents. This is consistent with our results that the peak longitudinal modulus in human lenses was constant up to the age of 45 to 50 years, whereas our earlier study of the murine lenses showed continually increasing longitudinal modulus over age.[24]

Finally, the Brillouin profiles of the left and right eyes of the same subject were nearly identical to each other. This result is in line with clinical findings that accommodation may be a consensual response, in which both eyes change equally to a change in accommodative stimulus.[60] In contrast, significant

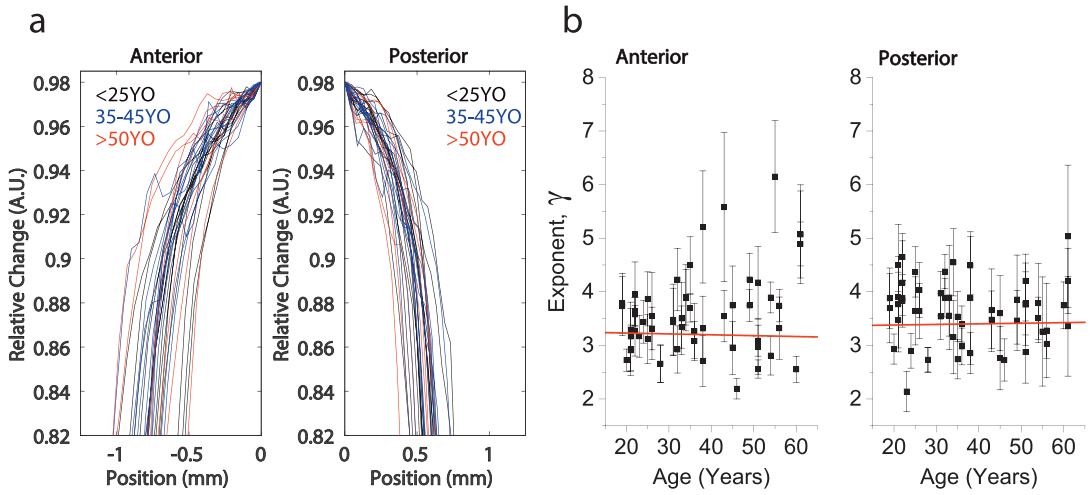

FIGURE 7. (**a**) Comparison of the cortical sagittal elasticity gradient between young (<25 years old), mid (35–45 years old), and old (>50 years old) groups. (**b**) Variation of the power law exponent for the cortical anterior and posterior regions. The *error bars* represent the 95% confidence bound of the fit coefficients.

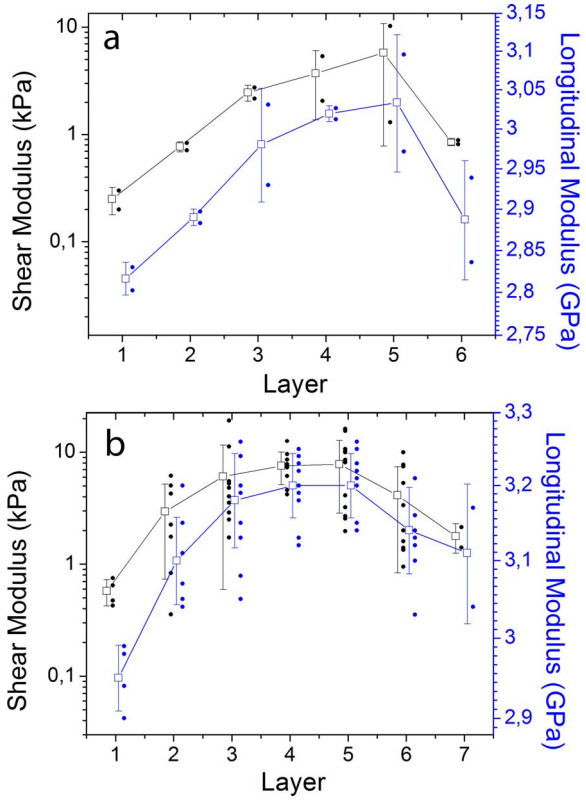

Figure 8. Spatial variation of the shear and longitudinal elastic moduli of ex vivo human lenses along the equatorial axis. (**a**) Young lenses (n = 2, 4-mm disks from the left and right eyes of a 26-year-old donor). (**b**) Old lenses (n = 4–8, 4-mm disks from left and right eyes of three donors at ages of 50, 60, and 62). *Solid dots*, measured data from each individual sample; *open squares*, average value of the data within each layer; and *error bars*, standard variation.

differences could be found in terms of lens thickness and elasticity in age-matched subjects within a 3-year window. Such differences could potentially explain the very broad range of accommodation amplitude observed at a given age.[1] In this regard, our approach would offer a unique tool to monitor mechanical changes resulting from surgical or pharmacological treatments.

Acknowledgments

The authors thank Mehron Puoris'haag for help in writing institutional review board protocols, and Peng Shao and Susana Marcos for helpful discussions.

Supported by the National Institutes of Health (R01EY025454 and R21EY023043), Harvard Catalyst Incubator program (UL1-RR025758), National Science Foundation (CBET-1562863 and CMMI-1537027), MGH Research Scholar award program, and the Natural Sciences and Engineering Research Council of Canada (NSERC) postdoctoral fellowship (to SB).

Disclosure: **S. Besner**, None; **G. Scarcelli**, None; **R. Pineda**, None; **S.H. Yun**, None

References

1. Duane A. Studies in monocular and binocular accommodation, with their clinical application. *Trans Am Ophthalmol Soc*. 1922;20:132–157.
2. Strenk SA, Semmlow JL, Strenk LM, Munoz P, Gronlund-Jacob J, DeMarco JK. Age-related changes in human ciliary muscle and lens: a magnetic resonance imaging study. *Invest Ophthalmol Vis Sci*. 1999;40:1162–1169.
3. Hermans EA, Pouwels PJW, Dubbelman M, Kuijer JPA, van der Heijde RGL, Heethaar RM. Constant volume of the human lens and decrease in surface area of the capsular bag during accommodation: an MRI and Scheimpflug study. *Invest Ophthalmol Vis Sci*. 2009;50:281–289.
4. von Helmholz HH. Handbuch der Physiologishen Optik. Leipzig: Leopold Voss; 1909.
5. Ostrin LA, Glasser A. Edinger-Westphal and pharmacologically stimulated accommodative refractive changes and lens and ciliary process movements in rhesus monkeys. *Exp Eye Res*. 2007;84:302–313.
6. Borja D, Manns F, Ho A, et al. Optical power of the isolated human crystalline lens. *Invest Ophthalmol Vis Sci*. 2008;49:2541–2548.
7. Glasser A, Campbell MCW. Presbyopia and the optical changes in the human crystalline lens with age. *Vision Res*. 1998;38:209–229.
8. Augusteyn RC, Mohamed A, Nankivil D, et al. Age-dependence of the optomechanical responses of ex vivo human lenses from India and the USA, and the force required to produce these in a lens stretcher: the similarity to in vivo disaccommodation. *Vision Res*. 2011;51:1667–1678.
9. Manns F, Parel JM, Denham D, et al. Optomechanical response of human and monkey lenses in a lens stretcher. *Invest Ophthalmol Vis Sci*. 2007;48:3260–3268.
10. Hugar DL, Ivanisevic A. Materials characterization and mechanobiology of the eye. *Mater Sci Eng C Mater Biol Appl*. 2013;33:1867–1875.
11. Fisher RF. Elastic constants of human lens. *J Physiol*. 1971;212:147.
12. Schachar RA, Chan RW, Fu M. Viscoelastic properties of fresh human lenses under 40 years of age: implications for the aetiology of presbyopia. *Br J Ophthalmol*. 2011;95:1010–1013.
13. Glasser A, Campbell MCW. Biometric, optical and physical changes in the isolated human crystalline lens with age in relation to presbyopia. *Vision Res*. 1999;39:1991–2015.
14. Heys KR, Friedrich MG, Truscott RJW. Presbyopia and heat: changes associated with aging of the human lens suggest a functional role for the small heat shock protein, alpha-crystallin, in maintaining lens flexibility. *Aging Cell*. 2007;6:807–815.
15. Heys KR, Cram SL, Truscott RJW. Massive increase in the stiffness of the human lens nucleus with age: the basis for presbyopia? *Mol Vis*. 2004;10:956–963.
16. Weeber HA, Eckert G, Pechhold W, van der Heijde RGL. Stiffness gradient in the crystalline lens. *Graefes Arch Clin Exp Ophthalmol*. 2007;245:1357–1366.
17. Wilde GS, Burd HJ, Judge SJ. Shear modulus data for the human lens determined from a spinning lens test. *Exp Eye Res*. 2012;97:36–48.
18. Pau H, Kranz J. The increasing sclerosis of the human lens with age and its relevance to accommodation and presbyopia. *Graefes Arch Clin Exp Ophthalmol*. 1991;229:294–296.
19. Hollman KW, O'Donnell M, Erpelding TN. Mapping elasticity in human lenses using bubble-based acoustic radiation force. *Exp Eye Res*. 2007;85:890–893.
20. Augusteyn RC. Growth of the lens: in vitro observations. *Clin Exp Optom*. 2008;91:226–239.
21. Reiss S, Sperlich K, Hovakimyan M, et al. Ex vivo measurement of postmortem tissue changes in the crystalline lens by Brillouin spectroscopy and confocal reflectance microscopy. *IEEE Trans Biomed Eng*. 2012;59:2348–2354.
22. de Korte CL, Vandersteen AFW, Thijssen JM, Duindam JJ, Otto C, Puppels GJ. Relation between local acoustic parameters and

protein distribution in human and procine eye lenses. *Exp Eye Res*. 1994;59:617–627.

23. Tsui PH, Huang CC, Chang CC, Wang SH, Shung KK. Feasibility study of using high-frequency ultrasonic Nakagami imaging for characterizing the cataract lens in vitro. *Phys Med Biol*. 2007;52:6413–6425.
24. Scarcelli G, Kim P, Yun SH. In vivo measurement of age-related stiffening in the crystalline lens by Brillouin optical microscopy. *Biophys J*. 2011;101:1539–1545.
25. Scarcelli G, Yun SH. In vivo Brillouin optical microscopy of the human eye. *Opt Express*. 2012;20:9197–9202.
26. Scarcelli G, Yun SH. Brillouin confocal microscopy for three-dimensional mechanical imaging. *Nat Photonics*. 2008;2:39–43.
27. Scarcelli G, Besner S, Pineda R, Kalout P, Yun SH. In vivo biomechanical mapping of normal and keratoconus corneas. *JAMA Ophthalmol*. 2015;133:480–482.
28. Wu C, Han Z, Wang S, et al. Assessing age-related changes in the biomechanical properties of rabbit lens using a coaligned ultrasound and optical coherence elastography system. *Invest Ophthalmol Vis Sci*. 2015;56:1292–1300.
29. Bailey ST, Twa MD, Gump JC, Venkiteshwar M, Bullimore MA, Sooryakumar R. Light-scattering study of the normal human eye lens: elastic properties and age dependence *IEEE Trans Biomed Eng*. 2010;57:2910–2917.
30. Scarcelli G, Yun SH. Multistage VIPA etalons for high-extinction parallel Brillouin spectroscopy. *Opt Express*. 2011;19:10913–10922.
31. Scarcelli G, Yun SH. Confocal Brillouin microscopy for three-dimensional mechanical imaging. *Nat Photonics*. 2008;2:39–43.
32. Scarcelli G, Kim P, Yun SH. Cross-axis cascading of spectral dispersion. *Opt Lett*. 2008;33:2979–2981.
33. Gross H, Blechinger F, Achtner B. Human eye. In: Gross H, ed. *Handbook of Optical Systems: Vol. 4 Survey of Optical Instruments*. Weinheim: WILEY-VCH Verlag GmbH & Co. KGaA, Weinheim; 2008:1092.
34. ANSI. American National Standards Institute Z136.1 - Safe Use of Lasers. Orlando, FL: The Laser Institute of America; 2014.
35. Delori FC, Webb RH, Sliney DH. Maximum permissible exposures for ocular safety (ANSI 2000), with emphasis on ophthalmic devices. *J Opt Soc Am A Opt Image Sci Vis*. 2007;24:1250–1265.
36. Sliney D, Aron-Rosa D, DeLori F, et al. Adjustment of guidelines for exposure of the eye to optical radiation from ocular instruments: statement from a task group of the International Commission on Non-Ionizing Radiation Protection (ICNIRP). *Appl Opt*. 2005;44:2162–2176.
37. Berghaus KV, Yun SH, Scarcelli G. High speed sub-GHz spectrometer for Brillouin scattering analysis. *J Vis Exp*. 2015;106:e53468.
38. Scarcelli G, Polacheck WJ, Nia HT, et al. Noncontact three-dimensional mapping of intracellular hydromechanical properties by Brillouin microscopy. *Nat Meth*. 2015;12:1132–1134.
39. Kasthurirangan S, Markwell EL, Atchison DA, Pope JM. In vivo study of changes in refractive index distribution in the human crystalline lens with age and accommodation. *Invest Ophthalmol Vis Sci*. 2008;49:2531–2540.
40. deCastro A, Siedleckib D, Borjacd D, et al. Age-dependent variation of the gradient index profile in human crystalline lenses. *J Mod Opt*. 2011;58:1781–1787.
41. Koretz JF, Strenk SA, Strenk LM, Semmlow JL. Scheimpflug and high-resolution magnetic resonance imaging of the anterior segment: a comparative study. *J Opt Soc Am A Opt Image Sci Vis*. 2004;21:346–354.
42. Atchison DA, Markwell EL, Kasthurirangan S, Pope JM, Smith G, Swann PG. Age-related changes in optical and biometric characteristics of emmetropic eyes. *J Vis*. 2008;8(4):29.
43. Augusteyn RC, Jones CE, Pope JM. Age-related development of a refractive index plateau in the human lens: evidence for a distinct nucleus. *Clin Exp Optom*. 2008;91:296–301.
44. Reiss S, Burau G, Stachs O, Guthoff R, Stolz H. Spatially resolved Brillouin spectroscopy to determine the rheological properties of the eye lens. *Biomed Opt Express*. 2011;2:2144–2159.
45. Randall J, Vaughan JM. The measurement and interpretation of Brillouin scattering in the lens of the eye. *Proc R Soc Lond B Biol Sci*. 1982;214:449–470.
46. Yoon S, Aglyamov S, Karpiouk A, Emelianov S. The mechanical properties of ex vivo bovine and porcine crystalline lenses: age-related changes and location-dependent variations. *Ultrasound Med Biol*. 2013;39:1120–1127.
47. Jones CE, Atchison DA, Meder R, Pope JM. Refractive index distribution and optical properties of the isolated human lens measured using magnetic resonance imaging (MRI). *Vision Res*. 2005;45:2352–2366.
48. Augusteyn R. Growth of the lens: in vitro observations. *Clin Exp Optom*. 2008;91:226–239.
49. Iribarren R. Crystalline lens and refractive development. *Prog Retin Eye Res*. 2015;47:86–106.
50. Van de Sompel D, Kunkel GJ, Hersh PS, Smits AJ. Model of accommodation: contributions of lens geometry and mechanical properties to the development of presbyopia. *J Cataract Refract Surg*. 2010;36:1960–1971.
51. Kasthurirangan S, Markwell E, Atchison D, Pope J. MRI study of the changes in crystalline lens shape with accommodation and aging in humans. *J Vis*. 2011;11(3):19.
52. Koretz L, Cook C, Kaufman P. Aging of the human lens: changes in lens shape at zero-diopter accommodation. *J Opt Soc Am A Opt Image Sci Vis*. 2001;18:265–272.
53. Dubbelman M, Van der Heijde G. The shape of the aging human lens: curvature, equivalent refractive index and the lens paradox. *Vision Res*. 2001;41:1867–1877.
54. Brown N. Change in lens curvature with age. *Exp Eye Res*. 1974;19:175–183.
55. Winn B, Whitaker D, Elliott D, Phillips N. Factors affecting light-adapted pupil size in normal human-subjects. *Invest Ophthalmol Vis Sci*. 1994;35:1132–1137.
56. Glasser A, Campbell MCW. Biometric, optical and physical changes in the isolated human crystalline lens with age in relation to presbyopia. *Vision Res*. 1999;39:1991–2015.
57. Jones CE, Pope JM. Measuring optical properties of an eye lens using magnetic resonance imaging. *Magn Reson Imaging*. 2004;22:211–220.
58. Zhao H, Chen Y, Rezabkova L, Wu Z, Wistow G, Schuck P. Solution properties of gamma-crystallins: hydration of fish and mammal gamma-crystallins. *Protein Sci*. 2014;23:88–99.
59. Siezen RJ, Wu E, Kaplan ED, Thomson JA, Benedek GB. Rat lens gamma-crystallins—characterization of the 6 gene-products and their spatial and temporal distribution resulting from differential synthesis. *J Mol Biol*. 1988;199:475–490.
60. Rosales P, Dubbelman M, Marcos S, van der Heijde R. Crystalline lens radii of curvature from Purkinje and Scheimpflug imaging. *J Vis*. 2006;6(10):5.